sciendo

ACTA CHEMICA IASI, **26_1**, 1-12 (2018)

DOI: 10.2478/achi-2018-0001

SYNTHESIS, STRUCTURAL AND ELECTRICAL STUDIES OF Li-Ni-Cu NANO FERRITES

Shashidhar N. Adarakatti[a], Veeresh S. Pattar[b], Prashant K. Korishettar[b], Bhagyashri V. Grampurohit[a], Ravindra G. Kharabe[b], Akshay B. Kulkarni[c], Shridhar N. Mathad[d*], Chidanandayya S. Hiremath[a], Rangappa B. Pujar[a]

[a]*P.G. Studies in Physics, P.C. Jabin Science College, Hubballi, Karnataka, India*
[b]*G.I.Bagewadi College, Nippani*
[c]*Jain College of Engineering, Belagavi, 590014, India*
[d]*K.L.E. Institute of Technology, Hubballi, 580030, India*

Abstract: Li-Ni ferrite has gained great scientific elicit owing to of its unparalleled properties and applications. The copper doped Li-Ni ferrite has been synthesized by sucrose method. The structure was characterized by X-ray diffraction, which has confirmed the formation of single-phase spinel structure. X-ray diffraction and FTIR data reveals the formation of cubic structure phase. Unit cell parameters vary with copper content; overall variation of the unit cell parameters obeys Vegard's law. The main absorption bands of spinel ferrite have appeared through IR absorption spectra recorded in the range of 300–700 cm^{-1}. The copper concentration dependence of lattice parameters obeys Vegard's law. DC electrical resistivity of the prepared samples decreases with increasing in the temperature which shows the semiconducting behaviour of all nano ferrites. The most prominent influence copper doping on the electrical properties of Li-Ni ferrites has been reported.

***Keywords*:** Ferrites, XRD, FTIR, Sucrose method, and electrical properties.

Introduction

Spinel ferrites have emerged as forefront materials in the field of material synthesis and engineering which is attributed due to tuning

[*]Shridhar.N.Mathad, *e-mail*: physicssiddu@gmail.com

properties and their vast applications. Ferrites are technologically primary materials that are used in the manufacturing of magnetic, electronic and microwave appliances. Some of their traditional applications include microwave devices, as contrast agents in magnetic resonance imaging (MRI), transformer applications, solar hydrogen production, sensors, catalysts, multi-layer chip inductors, high density magnetic recording, telecommunications, etc.[1-3] However, in recent years, many new avenues have opened and the latest research on spinel ferrites has developed in innumerable directions, increasing their potential applications to a much greater extent.[3-6] Chemical routes are used due to simple and economic way for producing homogenous ferrites with beneficial stoichiometry, homogeneity, narrow particle sized distribution, and high sinterability at low temperature.[7]

Lithium ferrites have become significant materials with their high resistivity, low dielectric losses, high Curie temperature, square hysteresis loop properties. Due to which they are used as microwave devices like circulators, isolators, and phase shifters.[8-10] Lithium ferrites altered by substitution with metal ions like, cobalt (Co^{2+}), nickel (Ni^{2+}), zirconium (Zr^{4+}), zinc (Zn^{2+}) and titanium (Ti^{4+}), etc. have been widely studied by many workers.[11] Ferrites can be synthesized by various routes like high-energy ball milling,[12] sol–gel technique,[13] micellar reactions,[14] sucrose method,[15] coprecipitation,[16] solid state method[17] and combustion synthesis.[18]

In this manuscript we established the properties of copper doped Li-Ni ferrite nano particles synthesized by sucrose method. The structural properties of ferrites have been explored by XRD. We have also thrown some light on electrical properties of ferrites by two probe method and influence of copper doing.

Experimental

The reagents used for the synthesis of $Li_{0.5}Ni_{0.75-X/2}Cu_{X/2}Fe_2O_4$ferrites were metal nitrates [(lithium nitrate, copper nitrate, nickel nitrate and iron nitrate (all A.R. Grade)] in required molar proportion distilled water to get homogenous solution. To this was added mixture of PVA and sucrose ($C_{12}H_{22}O_{11}$) solution prepared above and heated on a magnetic stirrer at suitable temperature to form a viscous mixture. This viscous mixture was then heated on an electric or gas heater till the powder began to burn like live charcoal undergoing oxidation to form nano ferrites. The ferrite powder was pre-sintered at 600 ^oC for 8 h in air .This powder was pressed into pellets which were subjected to final sintering at 800 ^oC for 6 h and cooled for homogenization of the composition of the raw materials, densification and grain growth simultaneously. The structural study of Li-Ni-Cu ferrites has been examined by XRD, FTIR and electrical studies by Two probe method.

Results and Discussion

The X-ray powder diffraction patterns of the $Li_{0.5}Ni_{0.75-X/2}Cu_{X/2}Fe_2O_4$Ferrites (x=0.0, 0.1, 0.3, 0.5, 0.7 and 0.9) ferrites are shown in Fig. 1. It is observed that all the peaks in the pattern belong to the cubic structure (spinel) and it is confirmed that the samples have pure spinel phase.[19] The diffraction pattern analysis by using (220), (311), (222), (440), (422), (511), (444) and (622) reflection planes confirms the cubic spinel structures. It is observed that as the concentration of Cu^{2+} ions enhances, the lattice parameter (a) also found increasing. The second order polynomial fit for the variation of lattice parameter (a) with composition (x) is given by

$$a = 0.000x^2 + 0.022x + 8.158 \quad (1)$$

This increase in lattice constant may be attributed to the increase in grain growth and increase in the concentration of the Cu^{2+} ions due to the relatively larger ionic radii of Cu^{2+} ions (0.72 A) in comparison to that of Li^{+} ions (0.71 A).

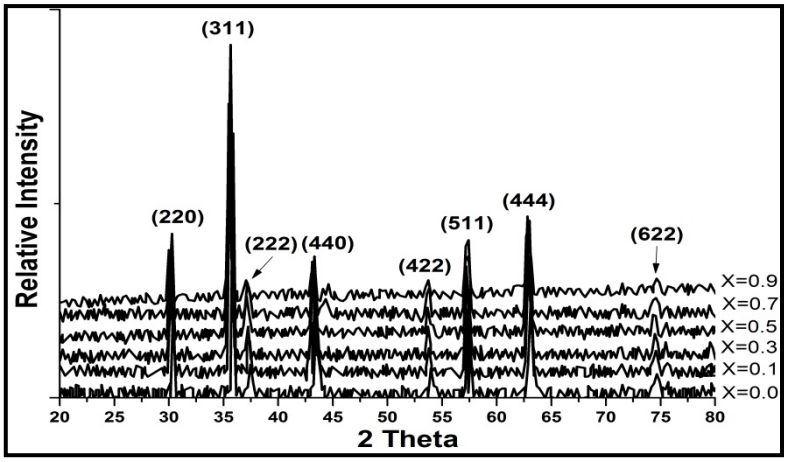

Figure 1. XRD patterns of $Li_{0.5}$ $Ni_{0.75-x}Cu_xFe_2O_4$ ferrite.

The average crystallite size of the prepared samples has been calculated using the following Debye– Scherrer's formula[15]

$$D = \frac{0.9\lambda}{\beta \cos\theta} \quad (2)$$

Lattice micro strain (ε) =βcosθ/4 (**3**)

The Williamson - Hall equation is used to calculate lattice strain, given by

$$\frac{\beta \cos\theta}{\lambda} = \frac{1}{D} + \frac{\varepsilon \sin\theta}{\lambda} \quad (4)$$

where ε is Lattice micro strain, D is average crystallite size, λ is the wavelength of X – Ray used, β is the Full Width Half Maximum and θ is the Bragg's angle.λ

From the graph slope is strain and reciprocal of intercept will be crystallite size of the sample. Comparative analysis of the parameter like crystallite size and strain found good agreements and Tabulated in Table 1.

Table 1. Comparison of Micro strain, crystallite sizes (W-H plot).

	From Equation		**From W-H graph**			
	Micro strain	**Crystallite size (A^0)**	**Intercept**	**Slope**	**Micro strain**	**Crystallite size (A^0)**
X=0.0	0.002953	906.94			0.001610	230.30
X=0.1	0.001688	291.52	0.00153	0.01181	0.001889	187.45
X=0.3	0.000503	261.82	0.00476	0.00675	0.001534	229.51
X=0.5	0.000475	223.81	0.00530	0.00201	0.001768	201.14
X=0.7	0.003810	963.63	0.00620	0.00190	0.001940	193.06
X=0.9	0.001765	267.36	0.00144	0.01524	0.002028	175.81

The dislocation is a crystallographic defect in a crystal structure. The dislocation density gives total number of dislocations (ρ_D) per unit volume of the material. The distance between magnetic ions (hopping length) in A site (Tetrahedral) and B site (Octahedral) were calculated by using the following relations:[15-16]

Dislocation Density

$$(\rho_D) = \frac{1}{D^2} \quad (5)$$

$$L_A = \frac{a \times \sqrt{3}}{4} \quad (6)$$

$$L_B = \frac{a \times \sqrt{2}}{4} \quad (7)$$

where a is lattice constant.

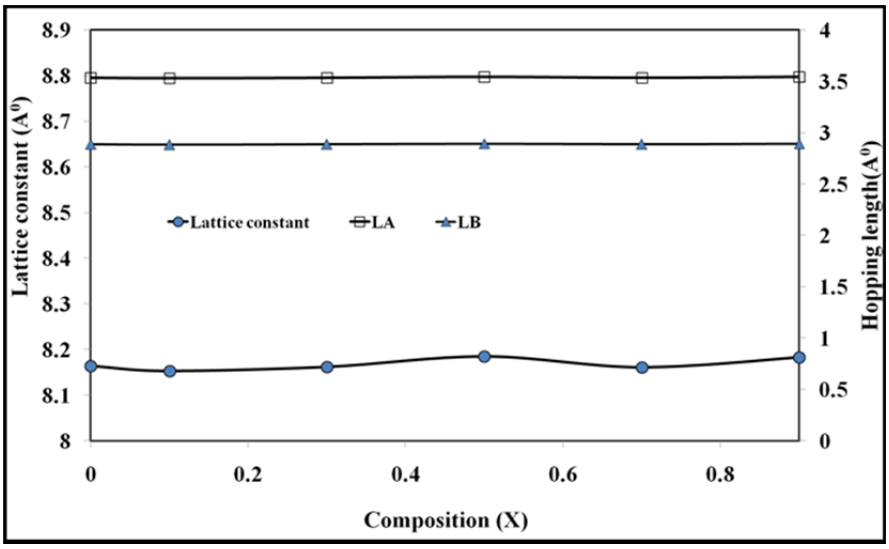

Figure 2. Variation of lattice parameter and hopping lengths with copper doping (x).

Dislocation density of ferrite samples lie in the range 0.1077 $X10^{15}$ to 1.459 $X10^{15}$. Lattice parameter, Hopping length, Volume and Dislocation density are tabulated in Table 2.

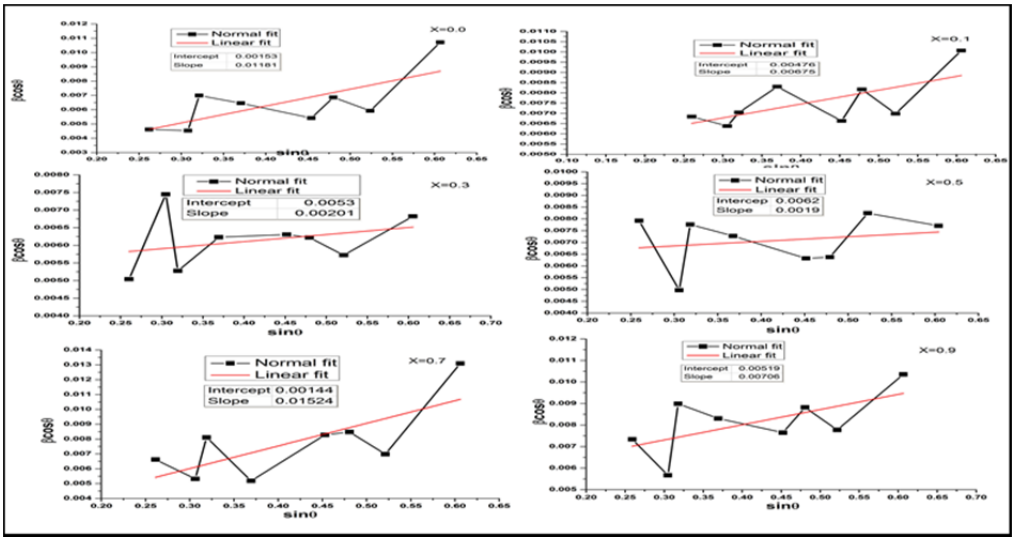

Figure 3. Williamson-Hall plots Ferrites.

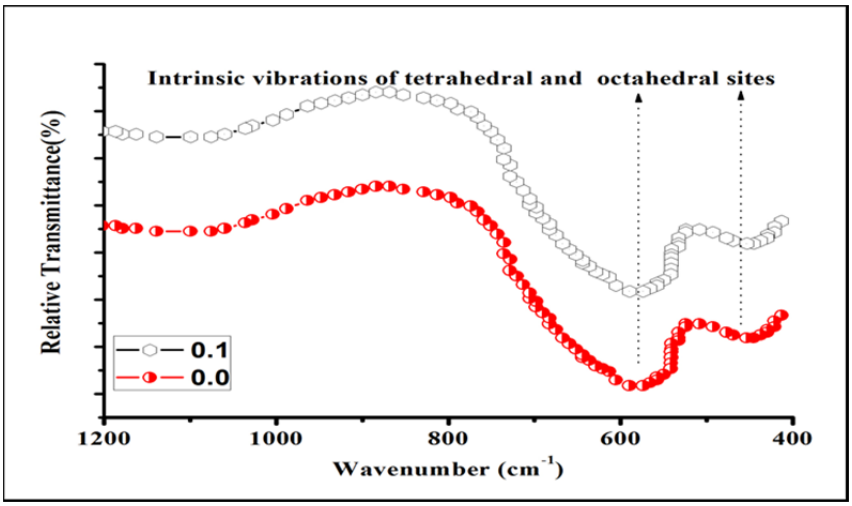

Figure 4. FTIR studies of $Li_{0.5}$ $Ni_{0.75-X/2}$ $Cu_{X/2}$ Fe_2O_4 Ferrites (X = 0.0 and X = 0.1).

Table 2. Lattice parameters, cell volume *V*, Hopping lengths, dislocation density, Curie temperature and Activation energy of Ferrite.

	Lattice parameter (A^0)	**Volume $(A^0)^3$**	**Hopping Lengths (A^0)**		**Dislocation density (ρ_D)**	**Curie temperature**	**Activation energy**
X	a (A^0)	V	L_A	L_B	X $10^{15}(m^{-2})$	Tc in K	(eV)
0.0	8.1635	544	3.5349	2.8862	0.1216	663	0.9402
0.1	8.1528	542	3.5303	2.8825	1.177	663	1.1102
0.3	8.1621	543	3.5343	2.8857	1.459	683	0.9412
0.5	8.1851	548	3.5443	2.8939	1.996	563	0.4013
0.7	8.1610	543	3.5338	2.8853	0.1077	593	1.0034
0.9	8.1829	548	3.5433	2.8931	1.399	603	0.8410

Figure 4 shows the IR spectra of the ferrite samples in the range from 400 to 700 cm^{-1}. Normal ferrites both absorption bands depend on the nature of octahedral M–O stretching vibration and nature of tetrahedral M–O stretching vibration. Two main frequency bands, namely, high frequency band (around 580 cm^{-1}) and low frequency band (around 430 cm^{-1}) reveals formation ferrite. These two observed bands (ν_1 and ν_2) correspond

to the intrinsic vibrations of tetrahedral and octahedral Fe^{3+}–O^{2} complexes, respectively.[15,17]

Electrical properties

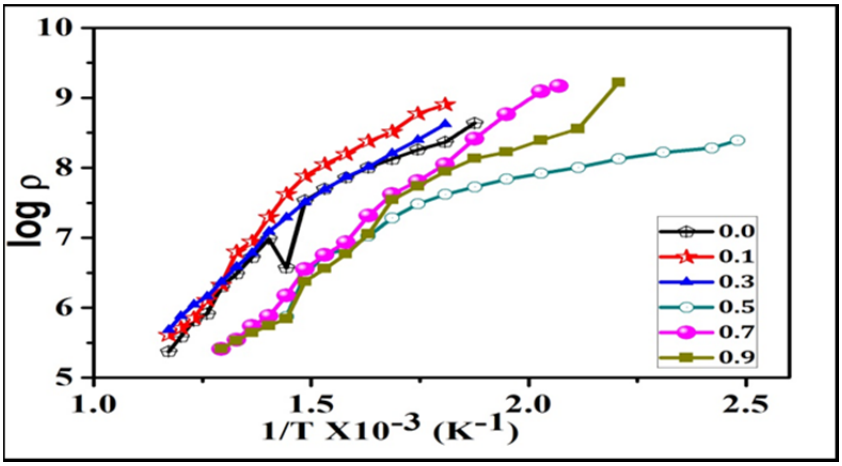

Figure 5. Variation of Electrical resistivity (ρ) of ferrites temperate (T).

The temperature-dependant of dc resistivity (log ρ Vs 1000/T) was measured as a function of temperature for all samples from room temperature to well beyond Curie temperature, which is described in Figure 5 follows Arrhenius plot. The change in the slope is observed in all the samples. Such a change is either due to Curie temperature or change in conduction mechanism.[10-11,13] The resistivity in Li-Ni-Cu ferrite materials decrease in with increasing temperature, evidences semiconducting nature. The conduction in ferrites is due to the hopping of electrons from Fe^{2+} to Fe^{3+}.[10-11,20-21] The discontinuity is caused by the ordering of Fe^{2+} and Fe^{3+} ions on the octahedral sites accomplished by a small change in crystal structure. The change in Curie temperature and activation energy (Table 2) is mainly due to spin ordering of electrons. Therefore it can be concluded that there is a predominant change in conduction mechanism due to magnetic phase transition. The electrical conductivity in ferrites can also be

explained on the basis of Verwey de Boer mechanism in which exchange of electrons takes place between the ions of same element that are present in more than two valence state and distributed randomly over equivalent crystallographic lattice sites. The number of such ions depends upon the sintering condition and reduction of Fe^{3+} ions into Fe^{2+} at elevated temperatures. The temperature at which magnetic transition takes place from ferrimagnetic to paramagnetic is known as Curie temperature. At Curie temperature, thermal randomization destroys magnetic ordering. Hence it plays an important role in microwave ferrite. According to Neel's model, Curie temperature is proportional to the product of Fe^{3+} ions on A and B sites and inter sub-lattice distances. The observed variation in Curie temperature may be due to cationic migration leading to fractional change of Fe^{3+} ion concentration at A and B sites. The value of activation energy lies in the range of 0.401-1.11 eV.[20-21]

The electrical properties are mainly governed by heat treatment during the preparation due to rapid dissociation of oxygen at elevated firing temperature. This leads to the formation of small amount of divalent ions and results in the increase of conductivity in ferrites. The presence of air gaps between the grains form in homogeneous structure. This largely affects D.C. conductivity and hence conduction mechanism in ferrites is largely dependent on porosity. Hence it can be emphasized that the higher conductivity in ferrites is the increase in grain diameter and decrease in pore concentration during the heat treatment. According to Neel's model, Tc is proportional to the product of Fe^{3+} ions on A and B sites and their inter sub lattice distances. The substitution of Cu^{2+} ions changes the concentration of Ni ions this increases the number of Fe^{3+} ions on both A and B sites. This results in the increase of curie temperature up to X = 0.3. There after Curie

temperature decreases with increase in Cu concentration. This is attributed to the decrease in Fe^{3+} ions on A and B sites, therefore it is concluded that the variation in Curie temperature with Cu concentration obeys Neel's model.[10-11,20-21]

Conclusions

In the report we have systematically reported the synthesized of Li-Ni-Cu ferrites by sucrose method. X-ray diffraction and FTIR data reveals the formation of cubic structure phase. Unit cell parameters vary with copper content; overall variation of the unit cell parameters obeys Vegard's law. Using W-H plots, micro stain and crystallite size has been compared. Dislocation density of ferrite samples lie in the range 0.1077 $x10^{15}$ to 1.459 $X10^{15}$. Dislocation density (ρ_D), crystallites and mechanical properties of Li-Ni-Cu ferrites for the first time. DC electrical resistivity of the prepared samples decreases with increasing in the temperature which shows the semiconducting behavior of nanoferrites. Thus we summarize the significant influence of the copper doping on the structure, mechanical and electrical properties and Li-Ni thick ferrites were reported.

References

1. Praveena, K.; Sadhana, K.; Bharadwaj, S.; Murthy, S.R. Development of nanocrystalline Mn–Zn ferrites for high frequency transformer applications. *J. Magn. Magn. Mater*. **2009**, *321*, 2433-2437.
2. Verma, A.; Alam,M.I.; Chatterjee, R.; Goel, T.C.; Mendiratta, R.G. Development of a new soft ferrite core for power applications. *J. Magn. Magn. Mater*. **2006**, *300*, 500-505.
3. Papazoglou, P.; Eleftheriou, E.; Zaspalis, V.T. Low sintering temperature MnZn-ferrites for power applications in the frequency region of 400 kHz. *J. Magn. Magn. Mater*. **2006**, *296*, 25-31.

4. Salunkhe, A.B.; Khot, V.M.; Thorat, N.D.; Phadatare, M.R.; Sathish, C.I.; Dhawale, D.S.; Pawar, S.H. Polyvinyl alcohol functionalized cobalt ferrite nanoparticles for biomedical applications. *Appl. Surf. Sci*. **2013**, *264*, 598-604.

5. Fresno, F.; Fernández-Saavedra, R.; Gómez-Mancebo, M.B.; Vidal, A.; Sánchez, M.; Rucandio, M.I.; Quejido, A.J.; Romero, M. Solar hydrogen production by two-step thermochemical cycles: Evaluation of the activity of commercial ferrites. *Int. J. Hydrogen Energy* **2009**, *34*, 2918-2924.

6. Kaneko, H.; Yokoyama, T.; Fuse, A.; Ishihara, H.; Hasegawa, N.; Tamaura, Y. Synthesis of new ferrite, Al-Cu ferrite, and its oxygen deficiency for solar H_2 generation from H_2O. *Int. J. Hydrogen Energy* **2006**, *31*, 2256-2265.

7. Dionne, G.F. Molecular-fielf coefficients of Ti^{4+} and Zn^{2+} substituted lithium ferrites. *J. Appl. Phys*. **1974**, *45*, 3621-3626.

8. Jadhav, S.A. Magnetic properties of Zn-substituted Li–Cu ferrites. *J. Magn. Magn. Mater*. **2001**, *224*, 167-172.

9. Al-Hilli, M.F.; Li, S.; Kassim, K.S. Gadolinium substitution and sintering temperature dependent electronic properties of Li-Ni ferrite. *J. Magn. Magn. Mater*. **2012**, *324*, 873–879.

10. Elata, A.M.A.; Attia, S.M.; Elkony, D.; Al-Hammadi, A.H. Spectral, initial magnetic permeability and transport studies of $Li_{0.5-0.5x}Co_xFe_{2.5-0.5x}O4$ spinel ferrite. *J. Magn. Magn. Mater*. **2005**, *295*, 28–36.

11. Sattar, A.A.; El-Sayed, H.M.; Agami, W.R.; Ghani, A.A. Magnetic properties and electrical resistivity of Zr^{4+} substituted Li-Zn Ferrite. *Am. J. Appl. Sci.* **2007**, *4*, 89-93.

12. Sepelak, V.; Bergmann, I.; Feldhoff, M.A.; Litterst, F.J.; Becker, K.D.; Cadogan, J.M.; Hofmann, M.; Hoelzel, M.; Wang, J.L.; Avdeev, M.; Campbell, S.J. Mechanosynthesis of nanocrystalline $MgFe_2O_4$: Neutron diffraction and Mössbauer spectroscopy. *Hyperfine Interact*., **2010**, *198*, 67–71.

13. Berchmans, L.J.; Selvan, R.K.; Kumar, P.N.S.; Augustin, C.O. Structural and electrical properties of $Ni_{1-x}Mg_xFe_2O_4$ synthesized by citrate gel process. *J.Magn. Magn. Mater*. **2004**, *279*, 103–110.

14. Iqbal, M.J.; Ahmad, Z.; Melikhov, Y.; Niebedim, I.C. Temperature and composition dependence of magnetic properties of cobalt–chromium co-substituted magnesium ferrite nanomaterials. *J. Magn. Magn. Mater*. **2012**, *324*, 3986–3990.

15. Rendale, M.K.; Mathad, S.N.; Puri, V. Structural, mechanical and elastic properties of $Ni_{0.7-x}Co_xZn_{0.3}Fe_2O_4$nano-ferrite thick films. *Microelectron. Intern*. **2017**, *34*, 57-63.

16. Yattinahalli, S.S.; Kapatkar, S.B.; Mathad, S.N. Structural and mechanical properties of a nano ferrite. *Adv. Sci. Focus*, **2014**, *2*, 42–46.

17. Patil, M.R.; Rendale, M.K.; Mathad. S.N.; Pujar, R.B. Structural and IR study of $Ni_{0.5-X}Cd_XZn_{0.5}Fe_2O_4$. *Int. J. Self-Propag. High-Temp. Synth*. **2015**, 24, 241–245.

18. Pathan, A.T.; Mathad, S.N.; Shaikh, A.M. Infrared Spectral studies of Co^{2+} substituted Li-Ni-Zn Nano-structured Ferrites. *Int. J. Self-Propag. High-Temp. Synth*. **2014**, 23, 112–117.

19. Singh, N.; Agarwal, A.; Sanghi, S.; Singh, P. Synthesis, microstructure, dielectric and magnetic properties of Cu substituted Ni–Li ferrites, *J. Magn. Magn. Mater*., **2011**, *323*, 486–492.

20. Aravind, G.; Raghasudha, M.; Ravinder, D. Electrical transport properties of nano crystalline Li–Ni ferrites. *J. Materiomics,* **2015**, *1*, 348–356.

21. Aravind, G.; Ravinder, D.; Nathanial, V. Structural and Electrical Properties of Li–Ni NanoferritesSynthesised by Citrate Gel Autocombustion Method. *Phys. Res. Intern*. **2014**, *Article ID 672739*.